Detection of the Horizontal Divergent Flow prior to the Solar Flux Emergence

S. Toriumi[1], K. Hayashi[2], and T. Yokoyama[1]

[1]Department of Earth and Planetary Science, University of Tokyo, 7-3-1 Hongo, Bunkyo-ku, Tokyo 113-0033

toriumi@eps.s.u-tokyo.ac.jp

[2]W. W. Hansen Experimental Physics Laboratory, Stanford University, Stanford, CA 94305, USA

Received _____; accepted _____

ABSTRACT

It is widely accepted that solar active regions including sunspots are formed by the emerging magnetic flux from the deep convection zone. In previous numerical simulations, we found that the horizontal divergent flow (HDF) occurs before the flux emergence at the photospheric height. This Paper reports the HDF detection prior to the flux emergence of NOAA AR 11081, which is located away from the disk center. We use SDO/HMI data to study the temporal changes of the Doppler and magnetic patterns from those of the reference quiet Sun. As a result, the HDF appearance is found to come before the flux emergence by about 100 minutes. Also, the horizontal speed of the HDF during this time gap is estimated to be 0.6 to 1.5 km s^{-1}, up to 2.3 km s^{-1}. The HDF is caused by the plasma escaping horizontally from the rising magnetic flux. And the interval between the HDF and the flux emergence may reflect the latency during which the magnetic flux beneath the solar surface is waiting for the instability onset to the further emergence. Moreover, SMART Hα images show that the chromospheric plages appear about 14 min later, located co-spatial with the photospheric pores. This indicates that the plages are caused by plasma flowing down along the magnetic fields that connect the pores at their footpoints. One importance of observing the HDF may be the possibility to predict the sunspot appearances that occur in several hours.

Subject headings: Sun: chromosphere – Sun: corona – Sun: photosphere – (Sun:) sunspots

1. Introduction

Solar active regions (ARs) including sunspots are generally thought to be the consequence of flux emergence, that is, the buoyant rise of the magnetic flux from the deep convection zone (Parker 1955). Observationally, the new emerging flux appears as a small and bright bipolar plage in the chromospheric Ca II H and K line cores (Fox 1908; Sheeley 1969). Soon afterwards, the arch filament system (AFS) composed of parallel dark fibrils appears in the line core of Hα (Bruzek 1967). The fibrils are magnetic field lines connecting the faculae of positive and negative polarities. In the photosphere, small pores are formed at the root of chromospheric filaments with downflows up to ~ 1 km s^{-1}. The faculae of opposite polarity separates, initially at the rate of > 2 km s^{-1}, and the rate drops to 1.3–0.7 km s^{-1} during the next 6 hours (Harvey & Martin 1973). New magnetic flux emerges continuously within the opposite polarities. If the flux is sufficient, the pores are gathered, and gradually sunspots are formed near the leading and the following plages (Zirin 1972).

In the last several decades, numerical computations have been well developed to reveal the dynamics of the flux emergence and the birth of the active region (e.g. Shibata et al. 1989). In our recent simulations on the large-scale flux emergence from a depth of $20,000$ km, the rising twisted flux tube in the convection zone decelerates and makes a flat structure just beneath the photosphere (e.g. Toriumi & Yokoyama 2012). In this calculation, the plasma, which is pushed up by the rising flux, escapes laterally around the surface. The appearance of the divergent outflow at the photosphere was found to be earlier than that of magnetic flux, and, at this moment, the outflow is mainly horizontal. Hereafter we call this preceding outflow as a horizontal divergent flow (HDF). A similar flow is also reported by Cheung et al. (2010). However, to our knowledge, the HDF prior to the flux emergence has not been confirmed clearly in previous observations (Kosovichev 2009).

Here, we use the term "horizontal" to indicate the direction parallel to the solar surface.

The aim of this study is to investigate the HDF and the evolving magnetic field at an early phase of the flux emergence. For this purpose, we used the Dopplergrams and magnetograms of the Helioseismic and Magnetic Imager (HMI) on board the Solar Dynamics Observatory (SDO), since their continuous observations of the whole solar disk make it possible to achieve information at the very moment of, or even before the flux emergence at the surface.

Our numerical result indicates that, if the newly emerging region is located away from the disk center, if a pair of positive and negative Doppler patterns is detected just before the flux emergence, and if the positive (negative) pattern is limbward (disk-centerward), the observed Doppler velocity is mainly horizontal rather than vertical. Therefore, we can evaluate the horizontal velocity of the escaping plasma from the Doppler velocity, by considering the heliocentric angle of the active region from the disk center. One advantage of this method over the ordinal local correlation-tracking method (November & Simon 1988) is that the horizontal velocity of the plasma can be evaluated independently of the apparent motion of magnetic elements at the photosphere. After the flux has emerged, we can not obtain the horizontal speed from the Doppler velocity, since it may contain a vertical motion such as rising of magnetic fields or a downflow in the convective collapse process.

In this Paper, we report the first determination of the HDF prior to the flux appearance, using SDO/HMI Dopplergrams and magnetograms. We also studied the chromospheric reaction to the flux emergence in the photosphere by using Hα images taken by the Solar Magnetic Activity Research Telescope (SMART) at Hida Observatory. In Section 2, we will introduce the observations and the method of data reduction. Analysis and the results will appear in Section 3. Then, in Section 4, we will discuss the observational results. Finally,

we will summarize the Paper in Section 5.

2. Observation and Data Reduction

In this Paper, we studied NOAA AR 11081 formed in 2010 June, in the northwest of the solar disk. To measure the Doppler shift and line-of-sight (LoS) magnetic field in the photosphere, we used Dopplergrams and magnetograms taken by SDO/HMI. Also, to study the chromospheric response to the flux emergence, we used Hα images taken by SMART at Hida Observatory.

2.1. SDO/HMI Dopplergram and Magnetogram

SDO/HMI continuously observes the whole solar disk at the 6173 ÅFe I line, which is resolved by 4096^2 pixels (Schou et al. 2012). To obtain the tracked data cubes of the birth of AR 11081, we used `mtrack` module [1]. The data cubes of the Doppler velocity and the LoS magnetogram have a spatial resolution of 0.5 arcsec (1 pixel corresponds to ~ 360 km) with 512^2 pixel field-of-view (FoV), and a temporal resolution of 45 s with a duration of 36 hr, starting at 12:00 UT on 2010 June 10. In the initial state, the center of the 512^2 FoV is located at N22° W25.6°, or $(+392, +383)$ arcsecs in solar disk coordinates. Here, we applied Postel's projection, that is, both Doppler and magnetic maps are projected as if seen from directly above. Then, to eliminate the effects of the rotation of the Sun and the orbital motion of the satellite, and to determine the zero point of the LoS velocity, we reduced the mean velocity from each Dopplergram. Also, a 30-min (40-frame) moving average was applied to the Dopplergrams and magnetograms.

[1] http://hmi.stanford.edu/teams/rings/mod_mtrack.html

Figure 1 is the HMI magnetogram of NOAA AR 11081 taken at 06:00 UT, 2010 June 11, that is, after the emergence started. Here, white and black indicate the positive and negative polarities, respectively. The diagonal line in this figure is the slit for the time-sliced diagram in Section 3.1. The slit angle is chosen to fit the first separating motion of both polarities. The square indicates the region analyzed in Section 3.2 to measure the distributions of the Doppler velocity and the LoS field strength.

2.2. SMART Hα Images

SMART at Hida Observatory, Kyoto University, consists of four different telescopes, which are T1, T2, T3 and T4, respectively (UeNo et al. 2004). They are placed on a tower with a height of 16 m. T1 obtains Hα full solar disk images at high temporal and spatial resolution. For studying the chromospheric reaction to the photospheric flux emergence, we analyzed the Hα data of 01:00–05:00 UT, 2010 June 11, which resolves the full solar disk with 4096^2 pixels (1 pixel corresponds to ~ 0.56 arcsec) and has a maximum temporal resolution of 2 minutes.

In this study, we only used Hα line core images (wavelength at 6562.8 Å). First, dark-current subtraction and flat fielding were performed on the obtained SMART data. Then, by taking a cross-correlation of the two consecutive images to fix the position of the target emerging active region, we made a data cube of Hα images. Note that Hα image is a simple zoom-up of the full disk image, while Postel's projection is applied to the HMI images.

3. Data Analysis and Results

Figure 2 shows the temporal evolution of the Dopplergram and the magnetogram for 12 hours from 18:00 UT, 2010 June 10. In the Dopplergram, the motion toward and away from the observer are shown in blue and red, respectively. At first, during 18:00–00:00 UT, the surface is relatively quiet with some preceding magnetic elements of both positive and negative polarities. An area with strong blue shift (< -1 km s^{-1}) appears in the middle of the FoV at 01:00 UT on 11 June, which is gradually growing in size. After 3:00 UT, the strong red shift (> 1 km s^{-1}) appears and magnetic field emergence takes place. Both positive and negative polarities move apart from each other. Here, the separation of the magnetic elements is almost along the slit, which is indicated as a diagonal line. Finally, at 06:00 UT, the red and blue areas become faint. The separated magnetic elements stop and gather to form pores at the boundary of the emerging region.

In this section, we first introduce the results of time-slices of the Dopplergrams and magnetograms in Section 3.1. Then, in Section 3.2, we will clarify the occurrence times of the HDF and the flux emergence, and evaluate the horizontal speed of the HDF. Section 3.3 is dedicated to showing the chromospheric studies.

3.1. Time-sliced Diagram

To examine the motion of the magnetic elements of positive and negative polarities and the corresponding LoS velocity, we made time-sliced diagrams of HMI Dopplergrams and magnetograms. The spatial slit is indicated as a diagonal line in Figure 1 and Figure 2, which is placed parallel to the separation of both polarities.

Figure 3 is the time-sliced diagram of the Dopplergram and the magnetogram along the slit. From the time-slice of the magnetogram, Figure 3(b), we can see that both positive

and negative polarities move apart from each other from around 03:00 UT on June 11. The speed of each element is estimated to be ~ 1.2 km s^{-1}, which then drops to ~ 0.4 km s^{-1}. Thus, the separation speed is 0.8–2.4 km s^{-1}. This deceleration of the separated polarities may reflect that the polarities are reaching the boundary of the active region. These elements then gathered to create stronger pores, of which the absolute LoS field intensity is greater than 200 G. One would find that weak and small elements of both polarities appear between the main separating pores during 03:00–09:00 UT on June 11. Also, the main positive pore collides with the preexisting negative polarity, and they cancel each other out.

In the Doppler slice, Figure 3(a), a pair of red and blue patterns emerged at around 02:00 UT, June 11, slightly earlier than the appearance of the magnetic elements in Figure 3(b). The red and blue shift patterns immediately started to separate, and the propagation speed of the patterns (the slope of the patterns) is about 0.4 km s^{-1}. Here, we note that the blue (red) pattern is located disk-centerward (limbward), which indicates that the flow is divergent. Moreover, from the fact that the divergent outflow came before the flux emergence, we can assume that the outflow during this period is caused by the plasma escaping from the rising magnetic flux. It should be noted that the trend of the Doppler pattern coming before the flux emergence does not change when we vary the thickness of the slit.

However, the determination of the appearance time of the Doppler pattern associated with the flux emergence is difficult, because the Doppler pattern, especially the blue shift, appeared at the location where the supergranulation showed blue shift (21:00–01:00 UT). The definition of the flux emergence and the appearance of the related Doppler pattern is dealt with in the next subsection (§3.2).

3.2. Appearance times of the HDF and the flux emergence, and the velocity of the HDF

It is not easy to determine the timings of the appearance of the HDF and the associated flux emergence from Figures 2 and 3. In particular, we have to distinguish the outflow related to the flux emergence from the preexisting convective motions of the quiet Sun (e.g., granulations and supergranulations). To clarify with significance when the HDF occurred and when the magnetic flux emerged, we studied the temporal changes of the Doppler and magnetic patterns from those before the emergence, namely, patterns of the quiet Sun. Also, in this subsection, we describe how we evaluate the horizontal speed of the HDF.

First, we plotted the histograms of the Doppler velocity and the absolute LoS field strength inside the square of Figure 1 for each frame. The size of the square is 70×70 pixels ($\sim 25 \times 25$ Mm^2), which is selected to include the emergence region. As for the Dopplergram, the apex of the histogram was shifted to fit the zero point. Then, considering the photospheric condition in the 3 hours from 21:00 UT of June 10 to be sufficiently quiet, we averaged up each 240 histograms of the Dopplergrams and the magnetograms in this period, and regarded these averages as reference quiet-Sun profiles.

In the left column of Figure 4, we show histograms of the Doppler velocity at five different times of June 11, plotted over the reference quiet-Sun profile. Here we note that the quiet-Sun profile obtained is similar to a Gaussian distribution. The shade indicates the standard deviation above and below the reference. As time goes by, the profile becomes deviated from the reference, because the number of pixels of which the absolute Doppler velocity is greater than 0.5 km s^{-1} increases. The right column of Figure 4 is the residual of the Doppler histogram from the reference. One standard deviation is also shown as a shaded area. At first, the residual is below one standard deviation level for most of the velocity range. From 02:00 UT, however, the residual exceeds the deviation.

Figure 5 is the same as Figure 4, but for the absolute field strength of the LoS magnetograms. Here, the quiet-Sun profile consists of a distribution with a width of ~ 10 G (about the precision of the HMI magnetogram) and some preexisting pores within the FoV. Thus, the profile is different from a Gaussian distribution. The residual in the range of > 200 G further exceeds one standard deviation level from 04:00 UT. After this time, the residual of > 200 G becomes well over the standard deviation, because more and more flux is emerged and stronger pores are created.

For the significance of the measurement, we define the start time of the HDF and the flux emergence as the time when each residual of the Dopplergrams and the magnetograms exceeded one standard deviation level. To know these times, we show in Figure 6 each time-evolution of the residuals (taken from and averaged over the range $[-0.8 \text{ km s}^{-1}, -0.4 \text{ km s}^{-1}]$ and $[0.4 \text{ km s}^{-1}, 0.8 \text{ km s}^{-1}]$ for Dopplergram, and the range $[200 \text{ G}, 300 \text{ G}]$ for magnetogram), plotted over one standard deviation. In this figure, the residual of the Dopplergram becomes over the standard deviation at 01:23 UT on 11 June, while that of the magnetogram exceeds the level at 03:06 UT. That is, the appearance of the HDF came before the flux emergence by about 100 minutes.

During this period, it is expected that the flow is mainly horizontal and a vertical component is less dominant. Thus, we can calculate the horizontal velocity from the residual distribution of the Doppler velocity (Figure 4), by considering the geometric effect. The relation between the horizontal velocity $V_{\rm h}$ and the Doppler velocity $V_{\rm D}$ is $V_{\rm h} = V_{\rm D}/\sin\theta$, where θ is the heliocentric angle of the emerging region measured from the disk center. From 01:23 to 03:06 UT, the Doppler velocity range where the residual exceeds the one standard deviation is typically 0.4–1.0 km s^{-1}, which is up to 1.5 km s^{-1}, and the heliocentric angle is $\sim 40^\circ$. Therefore, the horizontal velocity is calculated to be 0.6–1.5 km s^{-1}, and the maximum is 2.3 km s^{-1}.

Here, we comment on the selection of the field-strength range ([200 G, 300 G]) and its dependence on the start time of the flux emergence. If we use the lower strength range, for example [50 G, 100 G] or [100 G, 200 G], at which the residual exceeds one standard deviation level faster (Figure 5, right column), the start time of the flux emergence is calculated to be much earlier. In the present analysis, however, the strength range [200 G, 300 G] is used, since the number of the pixels of > 200 G is so small in the quiet Sun that the flux emergence is easily detected when it occurs. We confirmed this fact by applying the same analysis on the quiet-Sun data. As for the dependence of the strength range on the observation results, we tested the analysis with various ranges, which is summarized in Table 1. From this table one can see that the start time does not so change for [200 G, 300 G], [300 G, 400 G], and [400 G, 500 G] cases.

We also checked the dependence of the size of the square where the histograms are made (Fig. 1), which is summarized in Table 2. Here, the time difference is almost constant for various square sizes and is about 100 min. With increasing square size, the ratio of high-speed or strong pixels in the square reduces. At the same time, the quiet-Sun reference profile becomes more accurate and one standard deviation level decreases. Therefore, in total, the time difference remains constant.

3.3. Chromospheric Response

In this subsection, we investigate the time-evolution of the Hα intensity to examine the relation between the chromosphere and the photosphere in this studied event. Figure 7(a) is a sample image of the SMART Hα data. The color and contours indicate the relative Hα intensity. In this figure, there are two bright regions (plages) in the middle of the FoV. Then, along the slit of Figure 7(a), we made a time-sliced diagram for 4 hours starting at 01:00 UT, 11 June, which is shown as Figure 7(b). Note that the slit in Figure 7(a) is not

exactly the same as that in Figure 1, since the Hα data is a simple closeup view of the full disk image, while Postel's projection is applied to the HMI data. Thus, from this study, we can only determine the appearance time of the chromospheric brightening.

In Figure 7(b), the first bright source at the slit location of 5×10^4 km starts at 02:40 UT. However, it was found that this brightening is due to the activity among the preexisting quiet-Sun pores of both polarities, which later collide with positive patches of the newly emerging flux (see Section 3.1). It is difficult to separate this bright source into activity of the preexisting pores and that of the newly emerged positive pores. The second source located at 7×10^4 km starts at 03:20 UT, and there was no preceding pore in this region. Therefore, we consider that the second source is entirely due to the newly emerged negative pores, and determine that the chromospheric reaction starts at this time (03:20 UT; indicated by a dashed line in Figure 7(b)). The two chromospheric sources are located just over the positive and negative polarities in the photosphere.

4. Discussion

4.1. Mechanism of the Time Difference

In this Paper we analyze the newly emerging active region and find that there is a time difference between the appearance of the horizontal divergent flow (HDF) and the corresponding flux emergence; the HDF appears prior to the flux emergence by about 100 minutes.

According to the thin-flux-tube simulation (Fan 2009), the rising speed of the flux tube accelerates from the top few tens of Mm of the convection zone. However, at the same time, the flux tube expands as the external density (pressure) decreases with height. The radius of the tube eventually exceeds the local pressure scale height at a depth of ~ 20 Mm and

the thin-flux-tube approximation breaks out. Recently, our numerical simulations using the fully compressed MHD, including the convection zone, the photosphere, and the corona in a single computational box, have revealed that the rising flux tube decelerates in the uppermost convection zone (Toriumi & Yokoyama 2011, 2012). It is because the plasma on the flux tube piles up between the apex of the tube and the subadiabatically stratified photosphere ahead, and the plasma inhibits the rising motion of the flux tube. Then, the accumulated plasma in turn extends the tube laterally. This accumulation becomes effective from the depth where the apex of the tube becomes "flat". This critical depth is also considered as being where the tube's radius exceeds the local pressure scale height (depth ~ -20 Mm). The lateral expansion of the flux tube appears similar to those found by Magara (2001) and Archontis et al. (2004). However, their expansions occur because the tubes themselves move into the subadiabatic photosphere.

As the rising tube approaches the photosphere, the accumulated plasma on the rising tube escapes horizontally around the surface and is observed as an HDF, while the tube stops beneath the surface. Since the flux is continuously transported from below, the magnetic pressure gradient at the photosphere enhances and the further emergence to the upper atmosphere starts due to the magnetic buoyancy instability. When the flux resumes rising, it can be observed as a "flux emergence" at the photospheric level. Therefore, the time difference detected in this Paper implies the period of latency during which the flux tube reaching the photosphere develops the magnetic buoyancy instability. The growth time of the instability is, however, complicated and may be related to many parameters of the rising flux tube such as field strength, total flux, twist, etc. Thus, we shall leave the estimation of the time gap for our future numerical research.

4.2. Depth of the Magnetic Flux

To describe the relation between the HDF and the contributing upflow below the surface, we make a simple model, which is schematically illustrated as Figure 8. When the magnetic flux tube has emerged from the deeper convection zone, an upflow region is formed in front of the flux tube. If the typical size of this region is L and the velocity is $V_{\rm up}$, the mass flux passing through the area of πL^2 can be described as

$$F_1 = \rho_1 V_{\rm up} \pi L^2, \tag{1}$$

where ρ_1 is the plasma density. Next, the photospheric plasma that escapes from the upflow propagates the surface as an HDF. If we write the horizontal velocity at the radial distance r as $V_{\rm h}(r)$, the thickness as T, and the density as ρ_2, the mass flux passing through $2\pi rT$ is

$$F_2 = 2\pi r \rho_2 T V_{\rm h}(r). \tag{2}$$

These fluxes, F_1 and F_2, are assumed to be conserved. Therefore, from Equations (1) and (2), the upflow velocity is

$$V_{\rm up} = \frac{2\rho_2}{\rho_1} \frac{rTV_{\rm h}(r)}{L^2}. \tag{3}$$

As a result of the observational study, the horizontal speed is $V_{\rm h} \sim 1$ km s^{-1} at $r = 5000$ km. Here we assume that (a) plasma density is almost uniform around the photosphere, i.e., $\rho_1 \sim \rho_2$, (b) the thickness is about the local pressure scale height, $T \sim 200$ km, and (c) the size of the upflow is 4000 km (the smallest distance between the blue and red patterns in Figure 3); $L \sim 2000$ km. Under these assumptions, Equation (3) reduces to $V_{\rm up} = 0.5$ km s^{-1}. The time gap between the HDF appearance and the flux emergence was observed to be 100 min. Therefore, the depth that the apex of the magnetic flux transited across after it decelerated, is estimated to be ~ 3000 km, if the flux tube rises at the same rate as the upflow.

In this section, for simplicity, we assumed that the apex of the rising flux is circular, and that the outflow velocity $V_{\rm h}$ is only a function of r. From Figure 2, however, it seems that the HDF is not axisymmetric and is stronger in the direction of flux emergence (the northwest-southeast slit in this figure). This property is consistent with our preceding numerical results; the photospheric plasma flow is found to be along the direction of flux emergence (see Toriumi & Yokoyama 2012, Fig. 4). Moreover, in that simulation, the twist of the rising flux tube is stronger and the magnetic field at the tube's surface is almost perpendicular to the axis of the tube. In the later phase of the target AR of this Paper, the separation of positive and negative polarities shifted into the northeast-southwest direction, i.e., perpendicular to the diagonal line in Figure 2. Taking into account the previous numerical results, and considering that the observed NE-SW direction indicates the axis of the flux tube that forms this AR, we can think that the twist of this flux tube is tight, and therefore the flow is in the NW-SE direction.

4.3. Relations with Recent Observations: HDF as a precursor

Using SOHO/MDI, Grigor'ev et al. (2007) observed NOAA AR 10488 and found that upflows of matter with a high velocity ($\gtrsim 0.4$ km s^{-1}) preceded flux emergences by 8 and 13 min. Thus, the last ~ 10 min of the divergent Doppler pattern observed in our study that remained for 100 min, may contain the upward motion. However, for most of the period, the flow is expected to remain horizontal. Note that the upflow velocity of $\gtrsim 0.4$ km s^{-1} reported by Grigor'ev et al. (2007) may be the speed of a magnetic flux rising in the photosphere. As for the estimated velocity ($V_{\rm up} = 0.5$ km s^{-1}) in Section 4.2, this value indicates the emergence speed of a magnetic flux in the uppermost convection zone.

By means of time-distance helioseismology, Ilonidis et al. (2011) detected strong acoustic travel-time anomalies as deep as 65 Mm, 1 to 2 days before the flux rate reaches its

peak, and (in most cases) a few hours before the start of the flux appearance at the surface (see also Kosovichev & Duvall 2008; Kosovichev 2009). These anomalies are considered as signs of the rising magnetic flux. Taking account of our numerical simulations (e.g. Toriumi & Yokoyama 2012), it is consistent to interpret this helioseismic anomaly as a result of the effect similar to the plasma accumulation; external media may be perturbed or compressed by the rising motion of the magnetic flux. The importance of the helioseismic anomaly in Ilonidis et al. (2011) and the HDF in our study is that these phenomena occur prior to the flux emergence at the photosphere. That is, these are the precursors of the flux emergence. By combining two types of observations, sunspot appearances may be predicted in the near future.

4.4. Further Emergence to the Upper Atmosphere

In Section 3.3, we found that the Hα brightenings (plages) were located over the positive and negative pores in the photosphere. This indicates that the brightenings are caused by the plasma flowing down along magnetic loops that connect the photospheric magnetic elements (see Shibata et al. 1989, Figure 10). The appearance of the chromospheric source was at 03:20 UT on June 11, while the flux emergence was at 03:06 UT. If we assume the Hα formation height as 2000 km, the rise velocity of the magnetic field is ~ 2.5 km s^{-1}. This value is smaller than the observed speed of the chromospheric arch filament system (AFS) of ~ 20 km s^{-1} (e.g. Bruzek 1967), which implies that the actual rise speed is faster than 2.5 km s^{-1} and it takes some time to create Hα plage after the flux reaches the chromospheric height.

5. Summary

In this Paper, we have observed the horizontal divergent flow (HDF) prior to the flux emergence by using SDO/HMI Dopplergram and magnetogram. The presence of the HDF was predicted by our preceding numerical simulations (e.g. Toriumi & Yokoyama 2012). The HMI's continuous observation of the whole solar disk provides the means to analyze the earlier stage of the flux emergence. The summary of the observation is given as Table 3.

First, we made time-slices of Dopplergram and LoS magnetogram of NOAA AR 11081. From the magnetic slice, we found that the magnetic elements of positive and negative polarities separated from each other. The apparent speed of a single element was, at first, 1.2 km s^{-1}. The speed then dropped to 0.4 km s^{-1} and the elements gathered to create stronger pores of > 200 G. In the Doppler slice, a pair of blue and red pattern was observed to separate, slightly earlier than the flux emergence, and the blue (red) pattern was located disk-centerward (limbward). This indicates that the HDF appeared prior to the flux emergence. According to our previous numerical experiments, the outflow is mainly horizontal during the period from the appearance of the outflow to the emergence of the magnetic flux.

Secondly, we evaluated the times of the HDF appearance and the flux emergence. To determine these times with significance, we studied the temporal changes of the Doppler and magnetic patterns from those of the quiet Sun, and defined them as the times when each profile exceeded one standard deviation of its quiet-Sun profile. As a result, the Doppler profile was found to deviate from the quiet-Sun profile at 01:23 UT, 2010 June 11, while the magnetic profile deviated at 03:06 UT. Therefore, the time difference was about 100 minutes. Also, by considering the heliocentric angle, the horizontal speed of the HDF in this time gap was estimated to be 0.6–1.5 km s^{-1}, up to 2.3 km s^{-1}.

The creation of the HDF is due to the density accumulated on the apex of the flux

tube during its ascent in the convection zone. This accumulation occurs between the flattened apex of the rising flux tube and the subadiabatically stratified photosphere. The compressed plasma escapes horizontally around the photosphere, which was observed in this Paper. After the magnetic flux is sufficiently intensified, the magnetic buoyancy instability is triggered and the magnetic field restarts into the upper atmosphere, which was also seen as a flux emergence in this Paper. Therefore, the time difference of $\sim$ 100 min may reflect the latency during which the flux is waiting for the instability onset.

Applying a simple model of the horizontal flow and the corresponding upflow beneath the surface, we speculated that the depth of the magnetic flux is about 3000 km. Previously, SOHO/MDI found that an upflow preceded the flux emergence by about 10 minutes (Grigor'ev et al. 2007). This implies that the last $\sim$ 10 min of the divergent outflow may include the upward motion. Even so, for most of the period, the outflow remains horizontal.

Moreover, using Hα images taken by SMART, we studied chromospheric response to the flux emergence at the photosphere. The time-slice showed a pair of Hα plages, which started from 03:20 UT, that is, $\sim$ 14 min after the flux emergence. The location of these brightenings were just over the photospheric pores. Therefore, we speculated that these brightenings are caused by the plasma precipitating along the magnetic fields that connect photospheric pores of both polarities.

The time gap between the HDF occurrence and the flux emergence will be investigated in our future numerical study. As for the observational study, the statistical analysis on HDFs would be the next target. Another importance of observing HDF is that this phenomenon can be considered as a precursor, which may allow us to predict sunspot formation that occurs in several hours.

We thank the SDO/HMI team for data support and useful discussions. S.T. thanks

Dr. A. Kosovichev for arranging his stay at Stanford University. This work was supported by the JSPS Institutional Program for Young Researcher Overseas Visits, and by the Grant-in-Aid for JSPS Fellows. We are grateful to the GCOE program instructors of the University of Tokyo for proofreading/editing assistance. We also appreciate the thorough and helpful comments by the anonymous referee.

REFERENCES

Archontis, V., Moreno-Insertis, F., Galsgaard, K., Hood, A., & O'Shea, E. 2004, A&A, 426, 1047

Bruzek, A. 1967, Sol. Phys., 2, 451

Cheung, M. C. M., Rempel, M., Title, A. M., & Schüssler, M. 2010, ApJ, 720, 233

Fan, Y. 2009, ASP Conf. Ser., 416, 489

Fox, P. 1908, ApJ, 28, 253

Grigor'ev, V. M., Ermakova, L. V., & Khlystova, A. I. 2007, Astronomy Letters, 33, 766

Harvey, K. L., & Martin, S. F. 1973, Sol. Phys., 32, 389

Ilonidis, S. Zhao, J., & Kosovichev, A. 2011, Science, 333, 993

Kosovichev, A. G., & Duvall, Jr., T. L. 2008, ASP Conf. Ser., 383, 59

Kosovichev, A. G. 2009, Space Sci. Rev., 144, 175

Magara, T. 2001, ApJ, 549, 608

November, L. J., & Simon, G. W. 1988, ApJ, 333, 427

Parker, E. N. 1955, ApJ, 121, 491

Schou, J., Scherrer, P. H., Bush, R. I., et al. 2012, Sol. Phys., 275, 229

Sheeley, Jr., N. R. 1969, Sol. Phys., 9, 347

Shibata, K., Tajima, T., Steinolfson, R. S., & Matsumoto, R. 1989, ApJ, 345, 584

Toriumi, S., & Yokoyama, T. 2011, ApJ, 735, 126

Toriumi, S., & Yokoyama, T. 2012, A&A, 539, A22

UeNo, S., Nagata, S.-i., Kitai, R., Kurokawa, H., & Ichimoto, K. 2004, SPIE Conf. Ser., 5492, 958

Zirin, H. 1972, Sol. Phys., 22, 34

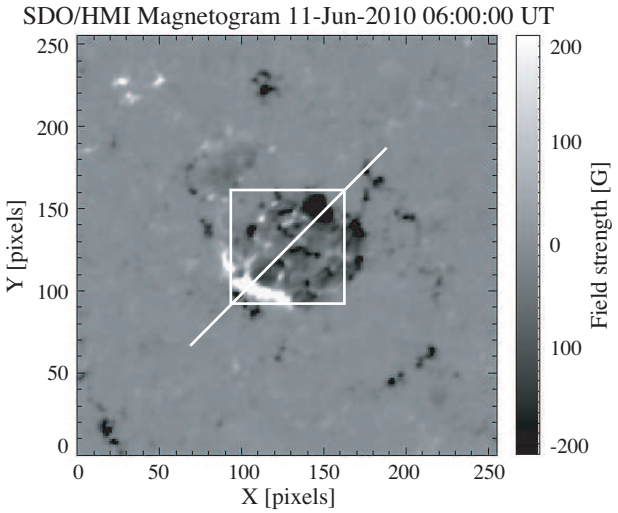

Fig. 1.— SDO/HMI magnetogram of NOAA AR 11081 taken at 06:00 UT on 2010 June 11. Positive and negative polarities are indicated by white and black, respectively. One pixel corresponds to $\sim$ 350 km. The diagonal line is the slit for time-sliced diagram (see Section 3.1). The square indicates the field in which temporal evolution of the Doppler velocity and the magnetic field strength (see Section 3.2) are analyzed.

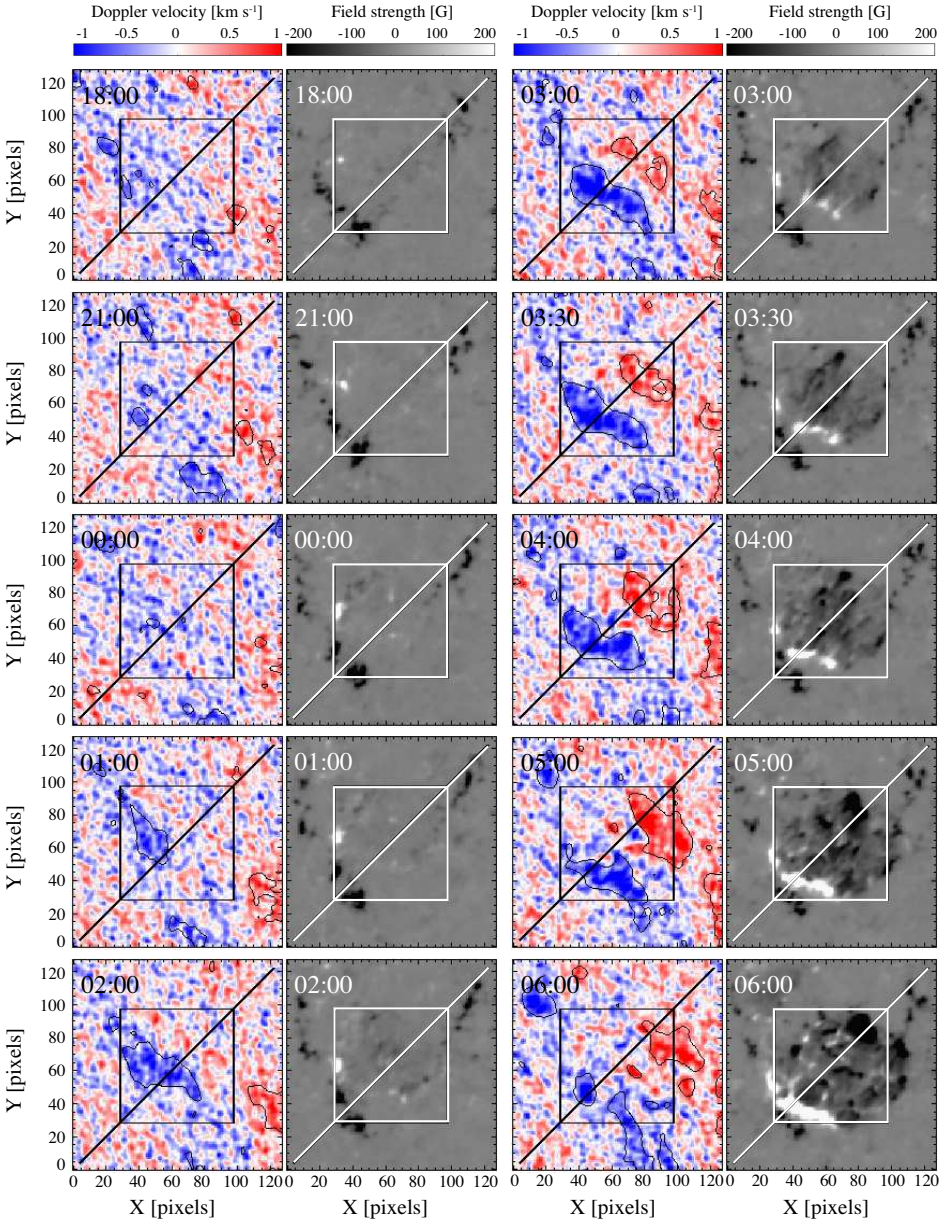

Fig. 2.— Temporal evolutions of the Dopplergram (red-blue map) and the magnetogram (white-black map) for 12 hours from 18:00 UT, 2010 June 10 to 06:00 UT, June 11. The diagonal line and the square in each panel are the slit for time-sliced diagrams (Section 3.1) and the field-of-view in which histograms are made (Section 3.2), respectively. In the Doppler maps, the motion toward and away from the observer are indicated in blue and red, respectively, and contours indicate the smoothed isolines of ± 1 km s^{-1}. In the magnetograms, positive and negative polarities are shown with white and black, respectively.

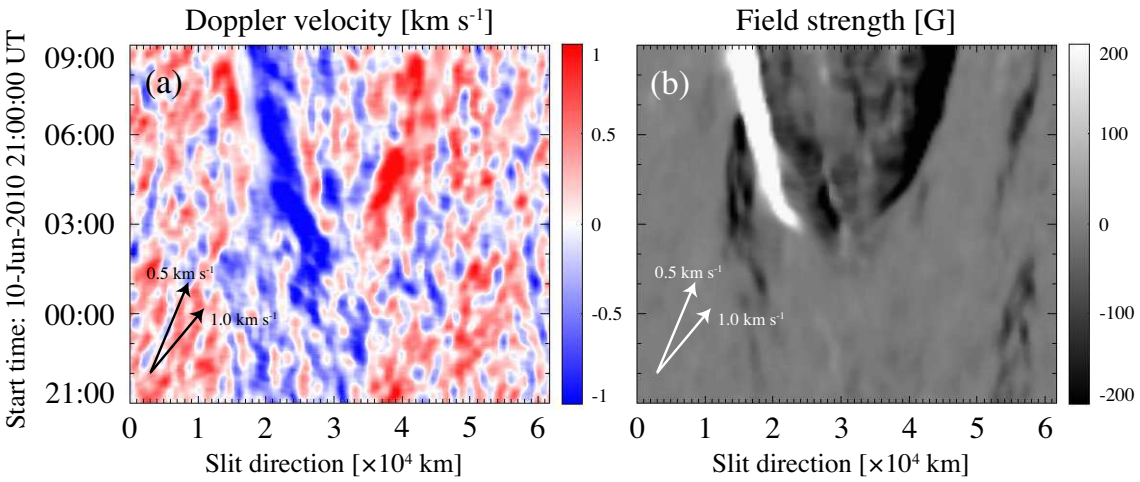

Fig. 3.— Time-slice diagram of (a) Dopplergram and (b) magnetogram along the slit shown in Figure 1 and Figure 2. Slit direction is selected limbward, i.e., the distance from the disk center increases with the horizontal axis. The duration of the time-slice is 12 hours, starting from 21:00 UT on 2010 June 10. In the Doppler time-slice (a), the motion toward (away from) the observer is indicated by blue (red) color. In the magnetogram time-slice (b), positive (negative) polarity is shown as white (black). Arrows give the apparent velocity.

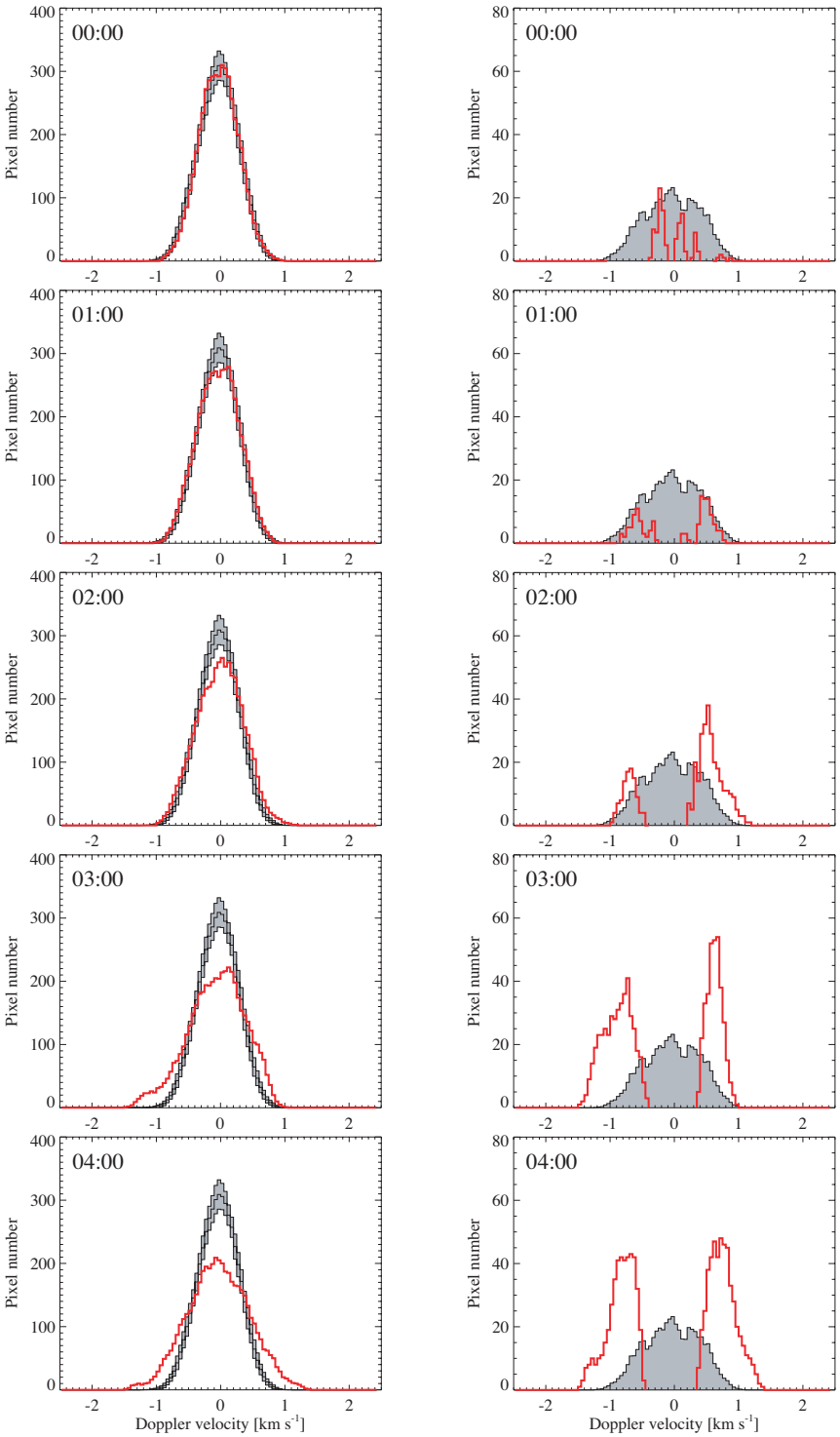

Fig. 4.— (*Left*) The histogram of the Doppler maps at five different times of 2010 June 11, indicated by red line, plotted over the quiet-Sun reference profile (middle black line). Shade indicates the standard deviation above and below the reference. (*Right*) The residual of the histogram from the reference, indicated by red line. Shade is one standard deviation level.

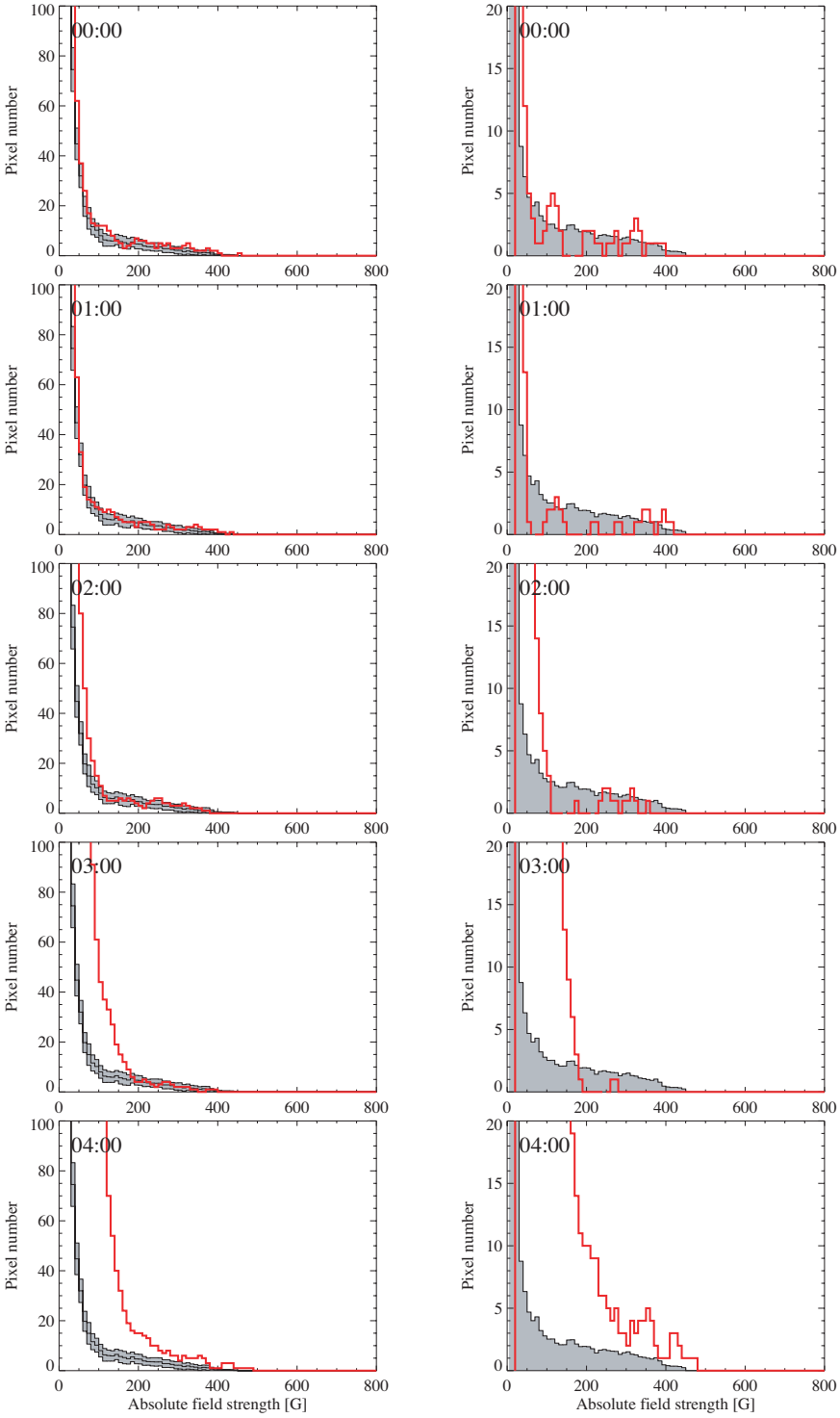

Fig. 5.— Same as Figure 4, but for the absolute field strength of the LoS magnetograms.

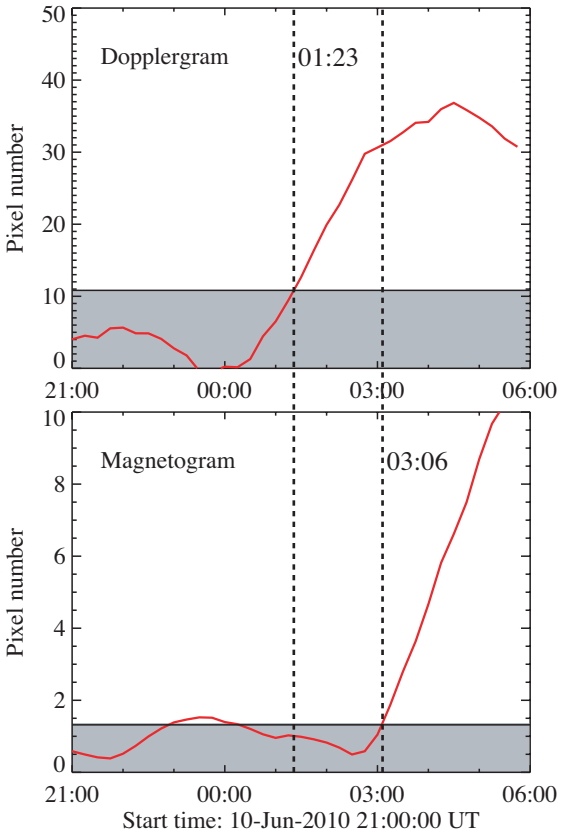

Fig. 6.— (*Top*) Time-evolution of the residual of the Doppler histogram (Figure 4), averaged over the range of $[-0.8\ \mathrm{km\ s^{-1}}, -0.4\ \mathrm{km\ s^{-1}}]$ and $[0.4\ \mathrm{km\ s^{-1}}, 0.8\ \mathrm{km\ s^{-1}}]$, starting from 21:00 UT, 2010 June 10. The shaded area is one standard deviation level. The residual exceeds the standard deviation level at 01:23 UT on June 11. (*Bottom*) The same for the magnetogram (Figure 5) over the range of $[200\ \mathrm{G}, 300\ \mathrm{G}]$. The residual exceeds at 03:06 UT.

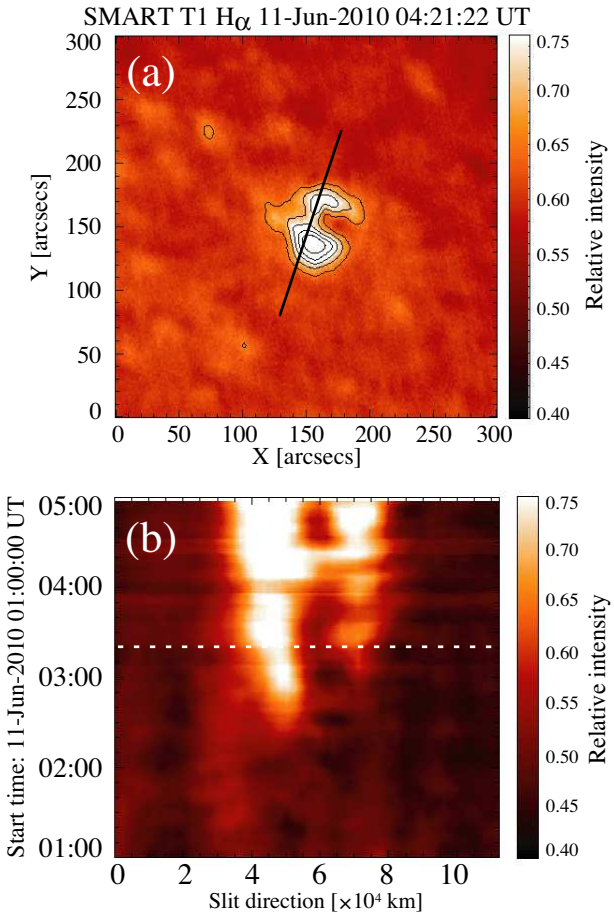

Fig. 7.— (a) A sample image of SMART chromospheric Hα data. The color and contours indicate the relative Hα intensity. Contour levels are 0.65, 0.70, 0.75, 0.80, and 0.85, respectively. The slit in the middle of the panel is used to make a time-sliced diagram. (b) Time-sliced diagram of Hα image for 4 hours from 01:00 UT, 2010 June 11. Color is the relative intensity. Slit direction (horizontal axis) starts from the bottom left of the slit in Panel (a). The dashed line indicates the time 03:20 UT (see text for details).

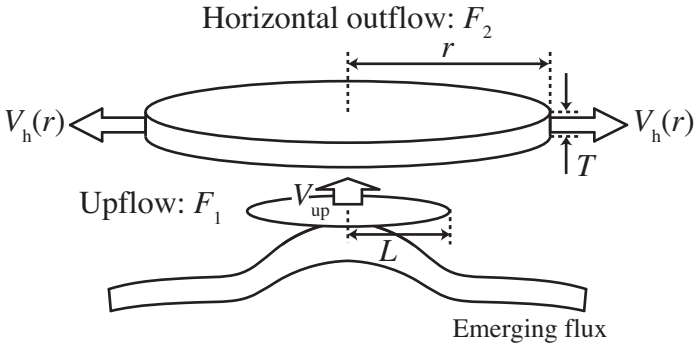

Fig. 8.— Schematic illustration of the model of flux emergence and the divergent horizontal flow. When the magnetic flux is emerged from the deeper convection zone, an upflow region with a size of L and a velocity of $V_{\rm up}$ is formed above the magnetic flux. At the photospheric level, the plasma is pushed away to create a divergent horizontal flow with a thickness of T. Here, r is the radial distance from the center of the emerging region and $V_{\rm h}(r)$ is the horizontal velocity at r. F_1 and F_2 are the mass fluxes of the upflow and the horizontal outflow, respectively.

Table 1. Dependence of the field-strength range

Field-strength range [G]	Start of flux emergence
0–50	-:- UT[a]
50–100	01:25 UT
100–200	02:15 UT
200–300[b]	03:06 UT
300–400	03:20 UT
400–500	03:25 UT
500–600	-:- UT[c]

[a]Residual is always below one standard deviation level

[b]Used in this Paper

[c]One standard deviation level is not defined

Table 2. Dependence of the square size

Square size [pixels]	HDF appearance	Start of flux emergence	Time difference [min]
50×50	01:00 UT	02:35 UT	95
60×60	01:25 UT	03:00 UT	115
70×70[a]	01:23 UT	03:06 UT	103
80×80	01:35 UT	03:15 UT	100
90×90	01:25 UT	03:20 UT	115
100×100	01:35 UT	03:20 UT	105
110×110	01:45 UT	03:05 UT	80
120×120	01:50 UT	03:05 UT	75

[a]Used in this Paper

Table 3. Summary of the AR 11081 observation

Physical value	Observational results
Field strength	< 500 G
Unsigned total flux	$\sim 10^{21}$ Mx
Region area	1.2×10^9 km^2
Appearance of horizontal outflow	01:23 UT[a]
Start of flux emergence	03:06 UT[a]
Start of chromospheric response	03:20 UT[a]
Time difference[b]	~ 100 min
Apparent speed[c]	$1.2 \rightarrow 0.4$ km s^{-1}
Horizontal velocity[d]	0.6–1.5 km s^{-1}
	(max 2.3 km s^{-1})

[a]On 11 June, 2010

[b]Time difference between the appearance of the horizontal outflow and the flux emergence

[c]Apparent speed of the magnetic elements

[d]Horizontal velocity of the surface plasma prior to the flux emergence